Invited Speaker

1208 Visualizing electronic correlations in quantum materials at millikelvin temperature
Prof Hermann Suderow[1]
[1]Laboratorio de Bajas Temperaturas y Altos Campos Magnéticos, Departamento de Física de la Materia Condensada, Instituto Nicolás Cabrera and Condensed Matter Physics Center (IFIMAC), Unidad Asociada UAM-CSIC, Universidad Autónoma de Madrid, E-28049 Madrid, Spain

Oral Presentation

7 EELS Compton scattering and the electronic structure of twisted WS2 bi-layers
Alina Talmantaite[1], Yaoshu Xie[2], Assael Cohen[3], Pranab Mohapatra[3], Ariel Ismach[3], Teruyasu Mizoguchi[2], Stewart Clark[1], Budhika Mendis[1]
[1]Dept of Physics, Durham University, , UK, [2]Institute of Industrial Science, University of Tokyo, , Japan, [3]3. Dept. of Materials Science and Engineering, Tel Aviv University, , Israel
423 Optical and acoustic plasmons in the layered material Sr2RuO4
Johannes Schultz[1], Axel Lubk[1,2], Fabian Jerzembeck[3], Naoki Kikugawa[4], Martin Knupfer[1], Daniel Wolf[1], Bernd Büchner[1,2], Jörg Fink[1,2]
[1]Leibniz Institute for Solid State and Materials Research, Dresden, Germany, [2]Institute of Solid State and Materials Physics, TU Dresden, Dresden, Germany, [3]Max Planck Institute for Chemical Physics of Solids, Dresden, Germany, [4]National Institute for Materials Science, Tsukuba 305-0003, Japan

Poster Presentation

68 Picometer-accurate Mapping of Lattice Displacements from Unconventional Room-Temperature Bond Order in Metallic NaRu2O4
Anna Scheid[1], Dr. Arvind Kumar Yogi[1,2], Mrs. Isha[1,2], Dr. Masahiko Isobe[1], Mrs. Birgit Bussmann[1], Dr. Tobias Heil[1], Prof. Dr. Peter A. van Aken[1]
[1]Max Planck Institute for Solid State Research, Stuttgart, Germany, [2]UGC DAE Consortium for Scientific Research, Indore, India
386 Modification of topological phenomena at hybrid Bi2Se3/organic interfaces
Miss Mairi McCauley[1], Dr. Timothy Moorsom[2], Professor. Quentin Ramasse[3], Dr. Craig Knox[4], Dr. Matthew Rogers[4], Professor. Donald MacLaren[1]
[1]SUPA, School of Physics and Astronomy, University of Glasgow, Glasgow, United Kingdom, [2]School of Chemical and Process Engineering, University of Leeds, Leeds, United Kingdom, [3]SuperSTEM Laboratory, SciTech Daresbury Campus, Daresbury, United Kingdom, [4]School of Physics and Astronomy, University of Leeds, Leeds, United Kingdom
675 Imaging the three-dimensional morphology of granular superconductors with energy-filtered TEM tomography
Lucas Brauch[1,4], Dr. Di Wang[2,3], Dr. Thomas Reisinger[1], Prof. Dr. Christian Kübel[2,3,4], Prof. Dr. Ioan Pop[1]
[1]Karlsruhe Institute of Technology, Institute for Quantum Materials and Technologies, Eggenstein-Leopoldshafen, Germany, [2]Karlsruhe Institute of Technology, Institute of Nanotechnology, Eggenstein-Leopoldshafen, Germany, [3]Karlsruhe Institute of Technology, Karlsruhe Nano Micro Facility, Eggenstein-Leopoldshafen, Germany, [4]Technical University of Darmstadt, Institute of Materials Science, Darmstadt, Germany

986 PFIB and SEM engineering of luminescent centres in hBN

Diane-Pernille Bendixen-Fernex De Mongex[2], Mr Mihai Vlad Ursta Anghel[1], Mr Amedeo Carbone[2,3], Associate Professor Nicolas Leitherer-Stenger[2,3], Senior Researcher Shima Kadkhodazadeh[1,6], Professor Thomas Willum Hansen[1]

[1]DTU Nanolab, Kgs. Lyngby, Denmark, [2]DTU Electro, Kgs. Lyngby, Denmark, [3]NanoPhoton – Center for Nanophotonics, Kgs. Lyngby, Denmark

1208

Visualizing electronic correlations in quantum materials at millikelvin temperature

Prof Hermann Suderow[1]
[1]Laboratorio de Bajas Temperaturas y Altos Campos Magnéticos, Departamento de Física de la Materia Condensada, Instituto Nicolás Cabrera and Condensed Matter Physics Center (IFIMAC), Unidad Asociada UAM-CSIC, Universidad Autónoma de Madrid, E-28049 Madrid, Spain

PS-10, Lecture Theater 5, august 26, 2024, 15:00 - 16:00

In this talk I will discuss the discovery of two-dimensional heavy fermions (2DHF) made of 5f electrons with an effective mass 17 times the free electron mass. These 2DHF present quantized states at terraces. The energy separation between quantized levels is of a fraction of a meV and the level width is set by the interaction with correlated bulk states [1]. Interestingly, we find a new connection between bulk and surface features. I will also describe recent new insight in the Josephson effect of ultra small Josephson junctions, which lead to an improved Josephson microscopy, called feedback Josephson microscopy.

[1] Quantum-well states at the surface of a heavy-fermion superconductor, Edwin Herrera, Isabel Guillamón, Víctor Barrena, William J. Herrera, Jose Augusto Galvis, Alfredo Levy Yeyati, Ján Rusz, Peter M. Oppeneer, Georg Knebel, Jean Pascal Brison, Jacques Flouquet, Dai Aoki & Hermann Suderow, Nature 616, pp 465-469 (2023).

7

EELS Compton scattering and the electronic structure of twisted WS2 bi-layers

Alina Talmantaite[1], Yaoshu Xie[2], Assael Cohen[3], Pranab Mohapatra[3], Ariel Ismach[3], Teruyasu Mizoguchi[2], Stewart Clark[1], Budhika Mendis[1]
[1]Dept of Physics, Durham University, , UK, [2]Institute of Industrial Science, University of Tokyo, , Japan, [3]3. Dept. of Materials Science and Engineering, Tel Aviv University, , Israel

PS-10, Lecture Theater 5, august 26, 2024, 15:00 - 16:00

Electronic structure is fundamental to a large class of materials phenomena, including mechanical, optical, magnetic and electronic transport properties. Momentum based spectroscopies such as angle resolved photoemission spectroscopy (ARPES), electron-positron annihilation and Compton scattering are traditionally used to measure the electronic structure. Compton scattering in the transmission electron microscope (TEM) was first explored in the 1980s using electron energy loss spectroscopy (EELS). Despite early success it did not achieve widespread use, largely due to the limitations in EELS spectrometer detector efficiencies, and artefacts arising from Bragg scattering within a crystalline specimen. However, with modern advances in EELS spectrometers as well as computational techniques for modelling dynamical scattering artefacts many of the challenges facing EELS Compton scattering are arguably now resolved. EELS Compton scattering in the TEM provides several benefits over standard X-ray and gamma-ray Compton measurements, such as a higher spatial resolution and the ability to extract useful information from even poly-crystalline materials.

In EELS Compton scattering the incident electron beam undergoes an inelastic collision with individual electrons in the solid. The Compton signal appears as a broad peak in an EELS spectrum acquired at large scattering angles (i.e. high momentum transfer). The width of the Compton profile, which can be as large as several hundred eV, is due to the intrinsic momentum spread of the solid-state electrons. The Compton profile shape is therefore directly related to J(pz), i.e. the density of solid-state electrons with momentum component pz along the scattering vector direction. J(pz) provides a 1D projection of the electronic band structure in reciprocal space. We have applied EELS Compton scattering to examine the electronic structure of bi-layer WS_2, with a twist angle of 18^o between the two layers. The twist angle and the resulting electronic structure is known to control the optical, vibrational and electrical properties of TMD bi-layers. EELS Compton scattering is particularly suitable to this problem, since the low dimensional nature of the WS_2 flakes make it difficult or impossible to analyse the electronic structure using conventional methods.

The J(pz) acquired along the 10-10 reciprocal direction indicates that the electrons are more delocalised in the bi-layer compared to monolayer WS_2. Comparison with density functional theory (DFT) simulations reveal that the delocalization is due to a small amount (i.e. 0.1%) of electronic charge accumulating in the inter-layer region (see figure; electron density is in grey, S atoms in yellow and top and bottom layer W atoms in blue and red respectively). The inter-layer charge accumulates between overlapping W atoms, thereby screening the ‘wrong’ bonds generated by the twist angle. The charge accumulation is also accompanied by a local dilation of the inter-layer spacing. The results uncover the precise nature of twist angle on the electronic and structural properties of bi-layer TMDs.

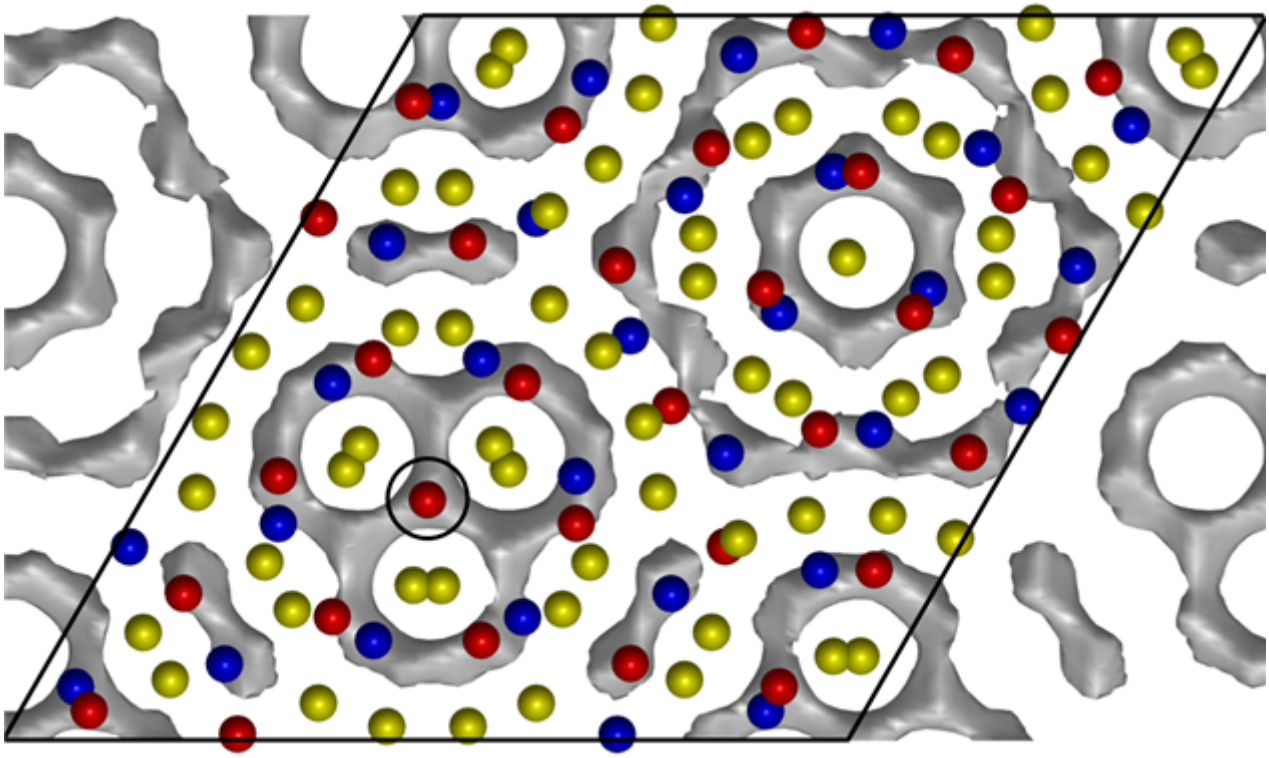

Keywords:

TMD, twist angle, EELS, Compton

423

Optical and acoustic plasmons in the layered material Sr2RuO4

Johannes Schultz[1], Axel Lubk[1,2], Fabian Jerzembeck[3], Naoki Kikugawa[4], Martin Knupfer[1], Daniel Wolf[1], Bernd Büchner[1,2], Jörg Fink[1,2]
[1]Leibniz Institute for Solid State and Materials Research, Dresden, Germany, [2]Institute of Solid State and Materials Physics, TU Dresden, Dresden, Germany, [3]Max Planck Institute for Chemical Physics of Solids, Dresden, Germany, [4]National Institute for Materials Science, Tsukuba 305-0003, Japan
PS-10, Lecture Theater 5, august 26, 2024, 15:00 - 16:00

Background incl. aims
In conventional metals, the conduction electrons show Fermi-liquid behavior with a characteristic quadratic dependence of the resistance on temperature. In contrast, in so-called “strange” metals the Fermi-liquid behavior breaks down due to strong correlation of the charge carriers, which has various consequences, e.g. a linear dependence of the resistance on the temperature. On the other hand, “strange” metals show unconventional and partially also high temperature superconductivity. Since the latter is supposed to be related to the non-Fermi-liquid behavior, the electronic structures of “strange” metals are of great interest in the field of solid state physics. Here we study the charge density-density response connected with plasmon excitations in the layered material Sr_2RuO_4, a representative of the class of “strange” metals [1]. We also wanted to test a theoretical prediction based on holography calculations [2] that plasmons in “strange” metals are overdamped.
Methods
Focused ion beam milling was used to prepare a lamella in which the layers are oriented perpendicular to the surface. This lamella was investigated using momentum resolved electron energy-loss spectroscopy (M-EELS) in a monochromized transmission electron microscope. Plasmon excitation in dependence on the momentum parallel and perpendicular to the layers was measured almost over the whole Brillouin zone [see Fig. 1 (a)] with a spectral and momentum resolution of 120 meV and 0.04 1/Å, respectively. The experimental data was compared to theoretical predictions of the Fetter model [3] and with the susceptibility χ_0 calculated from a tight binding band structure, all derived in terms of mean-field random-phase approximation.
Results
The M-EELS data show dispersing plasmon excitations below 1.8 eV with a continuous transition between the optical plasmon at qc=0 [purple squares in Fig. 1 (b)] and the acoustic plasmon at qc=0.4 1/Å [red squares in Fig. 1 (b)] close to the edge of the Brillouin zone at qc=0.49 1/Å. All curves are generally in good agreement with the theoretical calculations within the Fetter model taking into account a coupled system of 2D plasmons in the layered crystal structure. However, for qa ≥ qcrit there are differences between the theoretical curves and the experimental data, which can be explained by Landau damping [see open symbols in Fig. 1 (b)]. Here, qcrit is the momentum at which the dispersion curves merge into the single-particle-particle continuum χ_0 [see gray shaded regions in Fig. 1 (b)].
As predicted by the Fetter model, the measured dispersion at qc=0.4 1/Å extrapolates approximately to zero energy, which is characteristic for an acoustical plasmon. A fit of the experimental plasmon data to the Fetter model reveals that the dispersion is determined by the spacing of the layers and is only weakly influenced by many-body interactions.
Conclusion
The long wavelength qa dispersion of the qc dependent plasmons, including the optical and the acoustic collective excitations, resembles the data of the Fetter model, i.e., that of coupled 2D plasmons. Moreover, the critical momentum qcrit, at which the experimental data starts to deviate from the theoretical curves, agrees well with the calculated susceptibility χ_0. In summary, all data can be well explained within the framework of a mean-field random-phase approximation model. On the

other hand, we found no evidence supporting theories predicting an overdamped plasmon, i.e., a transition of the plasmon into a featureless, momentum-independent continuum already at very small momentum [2].

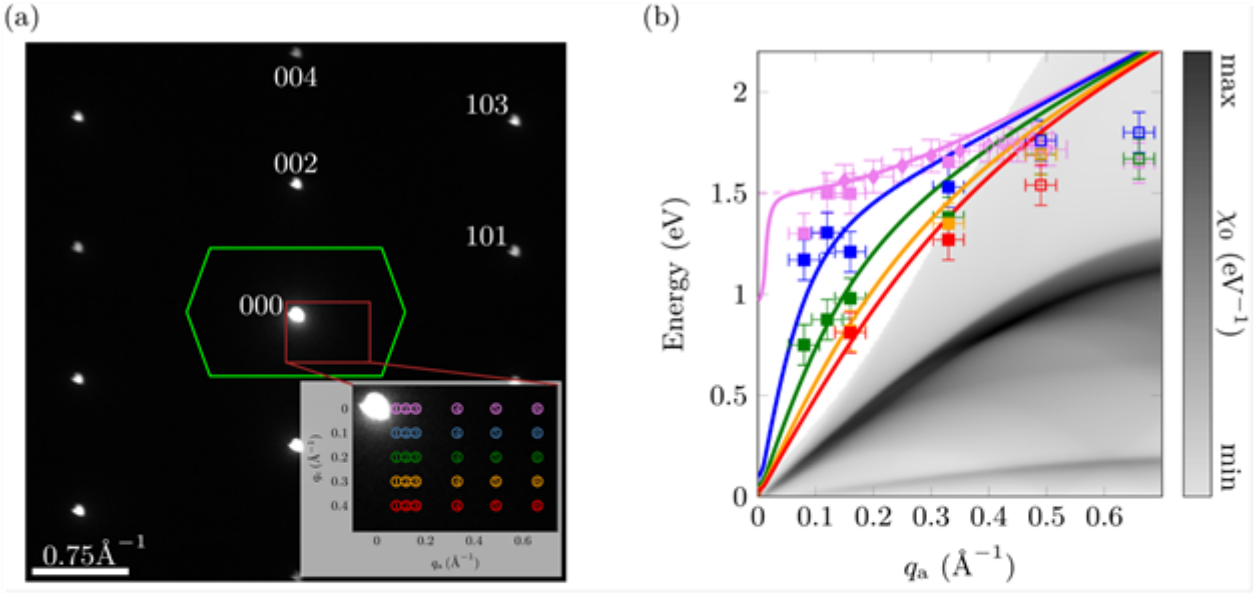

Fig. 1: (a) Indexed electron diffraction pattern in the (q_a, q_c) plane including the reduced Brillouin zone (green) for equally spaced layers along the c-axis. In the brown colored momentum range the loss spectra are recorded for various q_a and q_c values (see inset). The diameter of the colored circles in the inset corresponds to the diameter of the filter entrance aperture. (b) Plasmon dispersion along the momentum q_a parallel to the layers for several q_c perpendicular to the layers (squares) together with calculations within the framework of the Fetter model (solid lines). The q_c values 0, 0.1, 0.2, 0.3, and 0.4 Å^{-1} are marked by purple, blue, green, yellow, and red color squares, respectively. For comparison we added the optical plasmon dispersion (purple diamonds) derived in [4]. The region marked in gray corresponds to the susceptibility χ_0 calculated from a tight binding band structure. The excitations in the continuum range are marked by open symbols.

Keywords:

EELS, Plasmonics, Layered Materials

Reference:

[1] J. Schultz, A. Lubk, F. Jerzembeck, N. Kikugawa, M. Knupfer, D. Wolf, B. Büchner, and J. Fink, Optical and acoustic plasmons in the layered material Sr_2RuO_4, arXiv, 2401.05880 (2024).
[2] A. Romero-Bermúdez, A. Krikun, K. Schalm, and J. Zaanen, Anomalous attenuation of plasmons in strange metals and holography, PRB 99, 235149 (2019).
[3] A. L. Fetter, Electrodynamics of a layered electron gas. ii. periodic array, Annals of Physics 88, 1 (1974).
[4] M. Knupfer, F. Jerzembeck, N. Kikugawa, F. Roth, and J. Fink, Propagating charge carrier plasmons in Sr_2RuO_4, Phys. Rev. B 106, L241103 (2022).

68

Picometer-accurate Mapping of Lattice Displacements from Unconventional Room-Temperature Bond Order in Metallic NaRu2O4

Anna Scheid[1], Dr. Arvind Kumar Yogi[1,2], Mrs. Isha[1,2], Dr. Masahiko Isobe[1], Mrs. Birgit Bussmann[1], Dr. Tobias Heil[1], Prof. Dr. Peter A. van Aken[1]
[1]Max Planck Institute for Solid State Research, Stuttgart, Germany, [2]UGC DAE Consortium for Scientific Research, Indore, India

Poster Group 1

In recent years, there has been a remarkable increase in interest in ruthenium-based transition metal compounds, especially in the fields of quantum materials and strongly correlated electron systems. The reason for this is their moderate spin-orbit coupling, which is neither too weak nor too strong compared to the Coulomb interaction U. Due to this property, the relatively heavy 4d transition metal ruthenates exhibit a number of unusual properties compared to 3d transition metals. These include unconventional superconductivity, metal-insulator transitions, high-temperature ferromagnetism, Haldane chains, and orbital ordering. The interplay between localized and itinerant electrons, together with the orbital degrees of freedom in ruthenate systems, contributes to a wider range of electronic and magnetic properties [1, 2]. Given this potential of Na-Ru-O systems to serve as a promising model for the study of electron correlations in mixed-valence 4d systems, research in this area remains surprisingly limited.

$NaRu_2O_4$ exhibits an atypical metal-to-metal phase transition with emergent charge order (CO) [3]. Typically, a CO state, dominated by the inter-site energy U, tends to confine charge carriers to specific atomic positions, resulting in an insulating phase. Therefore, metallic behavior and charge ordering are generally considered to be mutually exclusive. Through single-crystal X-ray diffraction and theoretical studies, an unconventional type of bonding has been revealed in metallic $NaRu_2O_4$, involving an additional ordering of Ru3+/Ru4+ species. Below the critical temperature (TC = 535 K), a structural transition occurs from the high-temperature (HT) phase with the space group Pnma to the low-temperature (LT) phase with emergent superlattice reflections (0, ½, 0), which cannot be explained by the Pnma space group. Instead, the structure undergoes a transformation with a doubling of the unit-cell size and the formation of Ru-Ru metal dimers through orbital-driven Peierls dimerization. The final LT crystal structure of $NaRu_2O_4$ exhibits monoclinic symmetry with the space group P1121/a. Remarkably, short Ru-Ru dimers (bond-centered charge density wave) with direct metal-metal bonding coexist with metallic conductivity [3].

This study focuses on the investigation of the atomic-scale lattice reconstruction in the metallic $NaRu_2O_4$ system. High-angle annular dark-field scanning transmission electron microscopy (HAADF STEM) with atomic-resolution and electron diffraction techniques are used to reveal the structural transition with temperature, confirming the occurrence of orbital-driven Peierls dimerization as the sample temperature drops below TC. Periodic lattice displacement (PLD) maps further visualize the atomic displacement along different zone axes. The combination of (in-situ) HAADF STEM and Fourier processing allows for the mapping of phase transitions with complex displacement patterns in the picometer range, providing direct evidence for the bonding order in metallic $NaRu_2O_4$ (Figure 1).

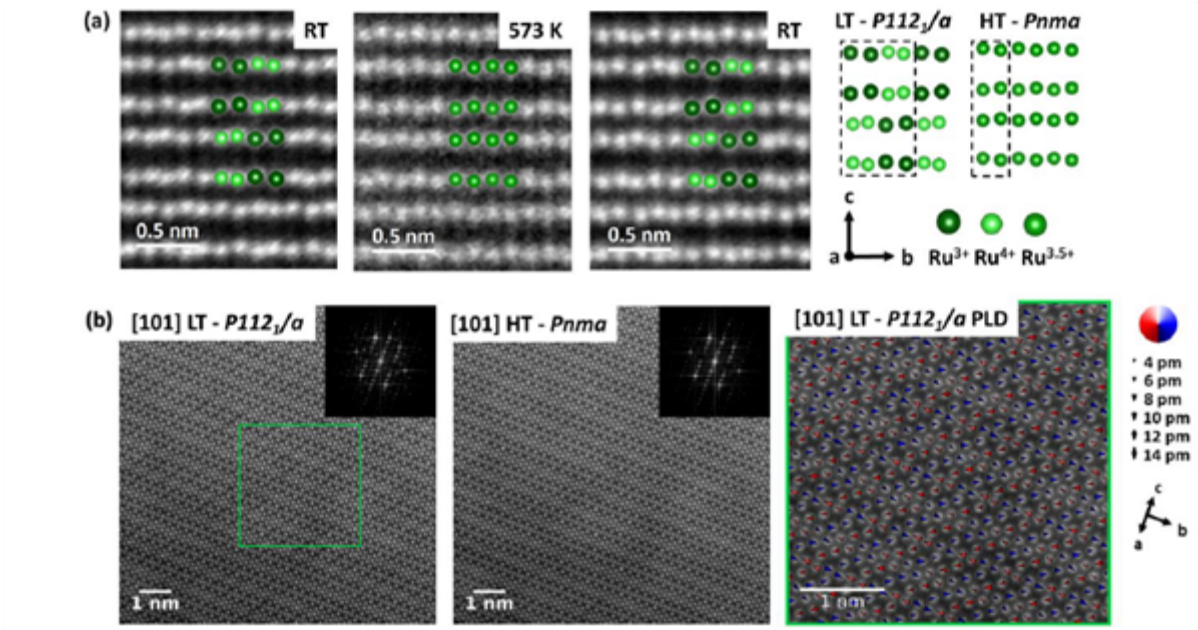

Figure 1. (a) Atomic-resolution *in-situ* HAADF STEM images of $NaRu_2O_4$ along the crystallographic [100] zone axis before heating, above T_C, and after cooling. The dashed black rectangles in the structural models in the bottom highlight the corresponding unit cells. Upon cooling below T_C, $NaRu_2O_4$ reorganizes back to LT-*P112₁/a*.
(b) Mapping of picometer-scale, periodic lattice displacements of Ru sites in $NaRu_2O_4$ oriented along the [101] zone axis. The synthetic HT-*Pnma* phase (middle) was obtained by Fourier transforming the original HAADF-STEM LT-*P112₁/a* image (left). In the Fourier transform, the amplitude of the (0, ½, 0) superlattice reflections was damped to the background level, while the phase was preserved. In the PLD map (right), colored arrows indicate the calculated ionic displacement. The arrow length represents the displacement amplitude and their color represents the polarization vector angle (the direction of the displacement).

Keywords:

phase transition, bond order, displacement

Reference:

1. C. Martins et al., J. Phys.: Condens. Matter, 29, 26 (2019).
2. T. Takayama et al. J. Phys. Soc. Jpn., 90, 6 (2021).
3. A. Yogi et al., Phys. Rev. B, 98, 8 (2018).
4. A. Yogi, et al., Commun Mater, 3, 1 (2022).

386

Modification of topological phenomena at hybrid Bi2Se3/organic interfaces

Miss Mairi McCauley[1], Dr. Timothy Moorsom[2], Professor. Quentin Ramasse[3], Dr. Craig Knox[4], Dr. Matthew Rogers[4], Professor. Donald MacLaren[1]
[1]SUPA, School of Physics and Astronomy, University of Glasgow, Glasgow, United Kingdom, [2]School of Chemical and Process Engineering, University of Leeds, Leeds, United Kingdom, [3]SuperSTEM Laboratory, SciTech Daresbury Campus, Daresbury, United Kingdom, [4]School of Physics and Astronomy, University of Leeds, Leeds, United Kingdom

Poster Group 1

Background
Topological insulators such as Bi_2Se_3 have interesting transport properties, including undamped transport via topologically-protected surface electronic states[1]. Manipulation of surface plasmons has been previously demonstrated using magnetic dopants, but these cannot be altered after growth. In contrast, the use of organic molecular overlayers such as C_{60} could be advantageous because it is possible to 'gate' the C_{60} interaction through electrical biasing and thereby develop tunable devices[2]. Here, we investigate plasmonic interactions at the interface of an as-deposited thin film sample of Bi_2Se_3/C_{60} using electron energy loss spectroscopy (EELS). We show changes in the characteristic plasmonic behaviour of the Bi_2Se_3 surface in the presence of C_{60}, providing greater understanding of the topological insulator-organic interface.
Methods
Bi_2Se_3 thin films were grown on a c-plane sapphire substrate by molecular beam epitaxy (MBE) with immediate subsequent deposition of C_{60} overlayers to avoid interfacial contamination. Cross-sections were extracted from the thin films by focused ion beam techniques and thinned to an electron transparent thickness of 35 nm for imaging. STEM and EELS were carried out on a mono-chromated instrument at 60 kV (the Nion UltraSTEMTM 100MC 'HERMES' instrument at the UK SuperSTEM facility).
Momentum-resolved EELS was used to map the plasmon dispersion with a convergence and collection semi-angles of 2 mrad and 1.1 mrad respectively. Spectra were collected containing only electrons scattered with specific momentum transfer from the lattice at momenta 0.0±0.3, 0.7±0.3, 1.0±0.3 and 1.4±0.3 1/Å along the ΓM direction of the first Brilliouin zone of Bi_2Se_3 to map the dispersion.
Results
EELS data and plasmon dispersions were obtained across two interfaces Al_2O_3/Bi_2Se_3 and Bi_2Se_3/C_{60} and are presented in figure 1. Panel is a HAADF STEM image of the stack, showing excellent film quality that includes clear crystallinity in the C_{60} layers. EELS spectra of bulk Bi_2Se_3 from the centre of the thin film (annotated blue in figure 1a) revealed two volume plasmons, at 7.2 and 17.3 eV, as well as two Bi core-loss edges between 25-28 eV (not shown). The dispersion of the 17.3 eV volume plasmon is shown in figure 1d and follows a parabolic trendline as expected from literature implying the classical nature of this plasmon.
A surface plasmon from Bi_2Se_3 was observed at 5 eV, localised to the Al_2O_3/Bi_2Se_3 interface, as shown in figure 1b. Its plasmon dispersion was observed to follow either a linear or root trend, plotted in figure 1e, which is similar to that predicted for π-electrons in graphene[3] and suggests the presence of a strongly confining interfacial potential. Comparison with simulations suggests that the nature of this surface plasmon could be a result of Bi_2Se_3 π-electrons confined in 2D to the surface[3]. The carrier density obtained from a fit of the surface plasmon dispersion concurs with the predicted number of carriers arising from Bi_2Se_3 π-electrons by DFT simulations.
At the other side of the thin film, additional features could be isolated as originating from interaction with C_{60} due to their absence at the Al_2O_3/Bi_2Se_3 interface. Across the Bi_2Se_3/C_{60} interface, the

surface plasmon energy was shifted higher in energy to 5.9 eV, shown in figure 1c. This interface contained features from bulk Bi_2Se_3 and C_{60} along with the additional surface plasmon. In bulk C_{60}, three interband transitions were observed, at 3.6, 4.7 and 5.8 eV, consistent with literature[4]; these exhibited very little dispersion with increasing momentum. At the Bi_2Se_3/C_{60} interface, some contribution of these non-dispersive interband transitions remained present. In momentum-resolved EELS spectra of this interface, dispersion of the observed surface plasmon was more difficult to map due to the additional spectral features present, however, the spectra could be decomposed into a linear combination of distinct contributions, revealing the presence of a dispersing feature, localised at the interface and that we identify as the interfacial plasmon.

Unusual plasmon dispersion of the Bi_2Se_3 surface plasmon was observed by momentum-resolved EELS similar to dispersion of 2D π-electrons in graphene. Upon fitting, an agreement in carrier concentration suggests the surface plasmon origin could be from the 2D confinement of Bi_2Se_3 π-electrons to the surface. Through the introduction of organic molecules such as C_{60}, the surface plasmon of Bi_2Se_3 was altered. Further work will characterise the interface between Bi_2Se_3 and other organic molecules such as H_2Pc.

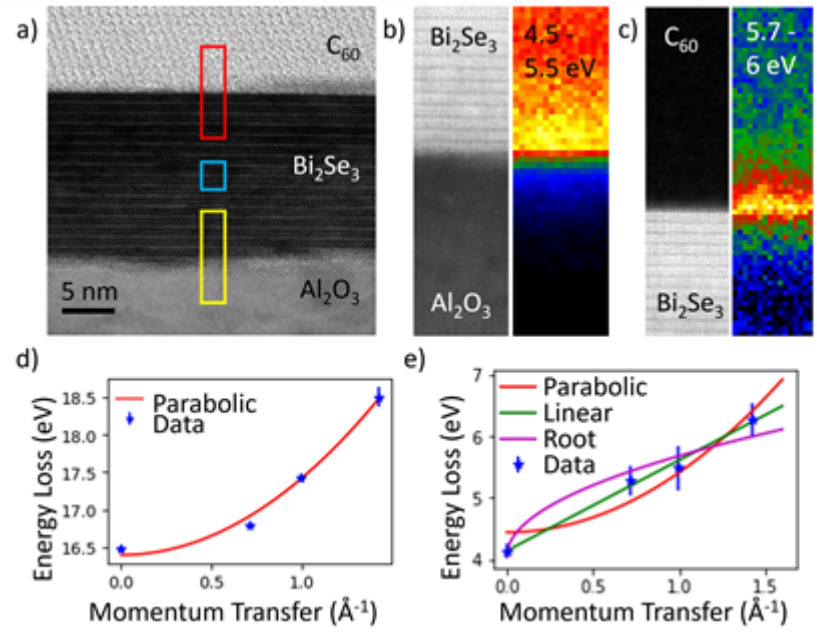

Figure 1: a) Bright field STEM image of a $Al_2O_3/Bi_2Se_3/C_{60}$ thin film with regions of EELS maps indicated in yellow and red for panels b and c, b) EELS spectrum image at 4.5 to 5.5 eV across the Al_2O_3/Bi_2Se_3 interface where increase intensity at the interface shows a surface plasmon. c) EELS spectrum image at 5.7-6 eV across the Bi_2Se_3/C_{60} interface with a surface plasmon. d) Plasmon dispersion of the bulk Bi_2Se_3 volume plasmon obtained via peak fitting of momentum resolved EELS spectra which follows a clear parabolic trend. e) Plasmon dispersion of the surface plasmon in b which follows a root or linear trend.

Keywords:

EELS, topological insulator, plasmons

Reference:

[1] Moore, J.E. (2010) Nature, 464(7286), pp. 194–198.
[2] Jakobs, S. et al. (2015) Nano Letters, 15(9), pp. 6022–6029.
[3] Liou, S.C. et al. (2015) Physical Review, 91(4).
[4] Hansen, P.L., Fallon, P.J. and Krätschmer, W. (1991) Chemical Physics Letters, 181(4), pp. 367–372.

675

Imaging the three-dimensional morphology of granular superconductors with energy-filtered TEM tomography

Lucas Brauch[1,4], Dr. Di Wang[2,3], Dr. Thomas Reisinger[1], Prof. Dr. Christian Kübel[2,3,4], Prof. Dr. Ioan Pop[1]
[1]Karlsruhe Institute of Technology, Institute for Quantum Materials and Technologies, Eggenstein-Leopoldshafen, Germany, [2]Karlsruhe Institute of Technology, Institute of Nanotechnology, Eggenstein-Leopoldshafen, Germany, [3]Karlsruhe Institute of Technology, Karlsruhe Nano Micro Facility, Eggenstein-Leopoldshafen, Germany, [4]Technical University of Darmstadt, Institute of Materials Science, Darmstadt, Germany

Poster Group 1

Background incl. aims
This work aims to resolve the structure - property relationship in granular Aluminum (grAl) thin films. GrAl is currently applied in microwave kinetic inductance detectors, parametric amplifiers, fluxonium qubits, resonators and filters. The granular structure and crystallite size distribution of the Aluminum particles have been known for a long time through dark field TEM imaging. The disadvantage of dark-field TEM is that it shows a 2D-projection of a 3D-network. In order to resolve the interconnection between the Al particles, 3D-STEM tomography was applied to resolve the morphology of the grAl. Combination with accurate models for simulations will advance the understanding of granular superconductors and their properties.
GrAl is produced by physical vapor deposition of Aluminum in presence of partial Oxygen pressure. It is a so-called 'dirty superconductor'. The emerging granular Aluminum nanostructure that is embedded in amorphous Aluminum oxide features tunable non linearity, kinetic inductance and low AC losses in its superconducting state. The Aluminum grains are assumed to form Josephson junctions between each other. A phase shift is induced on the superconducting current while tunneling through a small insulating Aluminum oxide gap between grains. Tunability of the non-linear properties is achieved by adjusting the room temperature resistivity of the film and varying the number of junctions in the network by changing the volume of a grAl component.
The critical temperature for superconductivity TC over the room temperature resistivity of the films reveals a dome shaped relationship with its maximum of 3 K at around 500 µΩcm while TC for pure aluminum is at 1.2 K. Depositing the films on cold substrates decreases Aluminum crystallite size and raises TC even beyond 3 K.
Methods
Two samples are investigated with 120 µΩcm and 25000 µΩcm resistivity. The films of 20 nm thickness are deposited on lacey Carbon TEM grids for easy nanowire templating. Gold fiducial markers are drop cast on the grid. The coated Carbon laces are investigated by energy-filtered TEM (EFTEM) on a Thermo Fisher Scientific Titan Themis Z at 80 kV with a Gatan image filter. EFTEM tomography was applied to reveal changes in al plasmon peak. The tilt series is aligned with the help of fiducial marker positions and is reconstructed using the Discrete Algebraic Reconstruction Technique (DART). Contrast levels are being estimated from an initial Simultaneous Iterative Reconstruction Technique (SIRT) reconstruction.
Results
STEM and TEM imaging show minimal contrast variations between Aluminum Oxide and metallic Aluminum due to similar atomic masses. Image corrected HRTEM shows partially polycrystalline grains in projection. EFTEM at 14 to 16 eV shows good contrast of the Aluminum volume plasmon which is confined to the Aluminum particles. Aluminum Oxide and Carbon give minimal intensity

contributions. The low resistivity sample with 120 µΩcm is reconstructed as a network of interconnected 5 nm Aluminum particles with a surface oxide cover of 3 nm. An oxide barrier separating close grains cannot be resolved. The non-linear inductive behavior can be explained with constrictions in the conductive path through the grains instead of oxide barriers as initially assumed. The high resistivity sample with 25000 µΩcm is reconstructed with 3 nm grains a notably bigger surface oxide layer of 12 nm. Many grains are still interconnected but there are oxide barriers separating clusters of grains from each other. The interconnection of grains at high resistivity is either a reconstruction artefact or shows that already a small amount of oxide barriers is sufficient for high non-linearity.

Conclusions

This study provides a novel insight into the 3D morphology of granular Aluminum (grAl) thin films, challenging previous assumptions about the structure-property relationship in these materials. The advanced electron microscopy techniques have revealed that the non-linear properties of grAl are more likely due to constrictions in the conductive path through the grains rather than oxide barriers. Furthermore, the study has shown that even a small number of oxide barriers can result in high non-linearity, particularly in high resistivity samples. These findings pave the way for more accurate simulations and could potentially enhance the performance of devices that utilize grAl. Further research is needed to fully understand the implications of these results and to explore the influence of substrate temperature during deposition on the structure of these films.

Keywords:

EFTEM Tomography Granular-Superconductor

Reference:

Grünhaupt, L., Spiecker, M., Gusenkova, D. et al. Granular aluminium as a superconducting material for high-impedance quantum circuits. Nat. Mater. 18, 816–819 (2019). https://doi.org/10.1038/s41563-019-0350-3

Deutscher, G., Fenichel, H., Gershenson, M. et al. Transition to zero dimensionality in granular aluminum superconducting films. J Low Temp Phys 10, 231–243 (1973). https://doi.org/10.1007/BF00655256

Rieger, D., Günzler, S., Spiecker, M. et al. Granular aluminium nanojunction fluxonium qubit. Nat. Mater. 22, 194–199 (2023). https://doi.org/10.1038/s41563-022-01417-9

986

PFIB and SEM engineering of luminescent centres in hBN

Diane-Pernille Bendixen-Fernex De Mongex[2], Mr Mihai Vlad Ursta Anghel[1], Mr Amedeo Carbone[2,3], Associate Professor Nicolas Leitherer-Stenger[2,3], Senior Researcher Shima Kadkhodazadeh[1,6], Professor Thomas Willum Hansen[1]
[1]DTU Nanolab, Kgs. Lyngby, Denmark, [2]DTU Electro, Kgs. Lyngby, Denmark, [3]NanoPhoton – Center for Nanophotonics, Kgs. Lyngby, Denmark

Poster Group 1

Hexagonal Boron Nitride (hBN) is a wide-band gap two-dimensional material, which has attracted much attention due to its ability to host luminescent centres with remarkable stability and single-photon in nature. This work explores the generation and characterization of luminescent centers in hBN on a SiO2/Si substrate using irradiation with a Scanning Electron Microscope (SEM) and Focused Ion Beam (FIB). We have investigated the impact of irradiation parameters on the optical and morphological properties as well as reproducibility of the luminescent centers using Photoluminescence (PL) spectroscopy, Atomic Force Microscopy (AFM), and SEM imaging. Our findings demonstrate the successful engineering of VB- centres, consistent with existing literature. We highlight the crucial role of material processing, such as the growth and annealing conditions of hBN and irradiation-specific parameters. This optimized methodology holds promise for generating B centres in hBN in a reproducible manner, providing a robust benchmark for future research in quantum technologies and other related fields.

Figure: a) Post PL map (left) and corresponding spectra from hBN flake treated with PFIB oxygen beam at different beam energies and doses. B) Post PL map (left) and corresponding spectra from hBN flake treated with the electron beam at 15 keV energy and different doses.

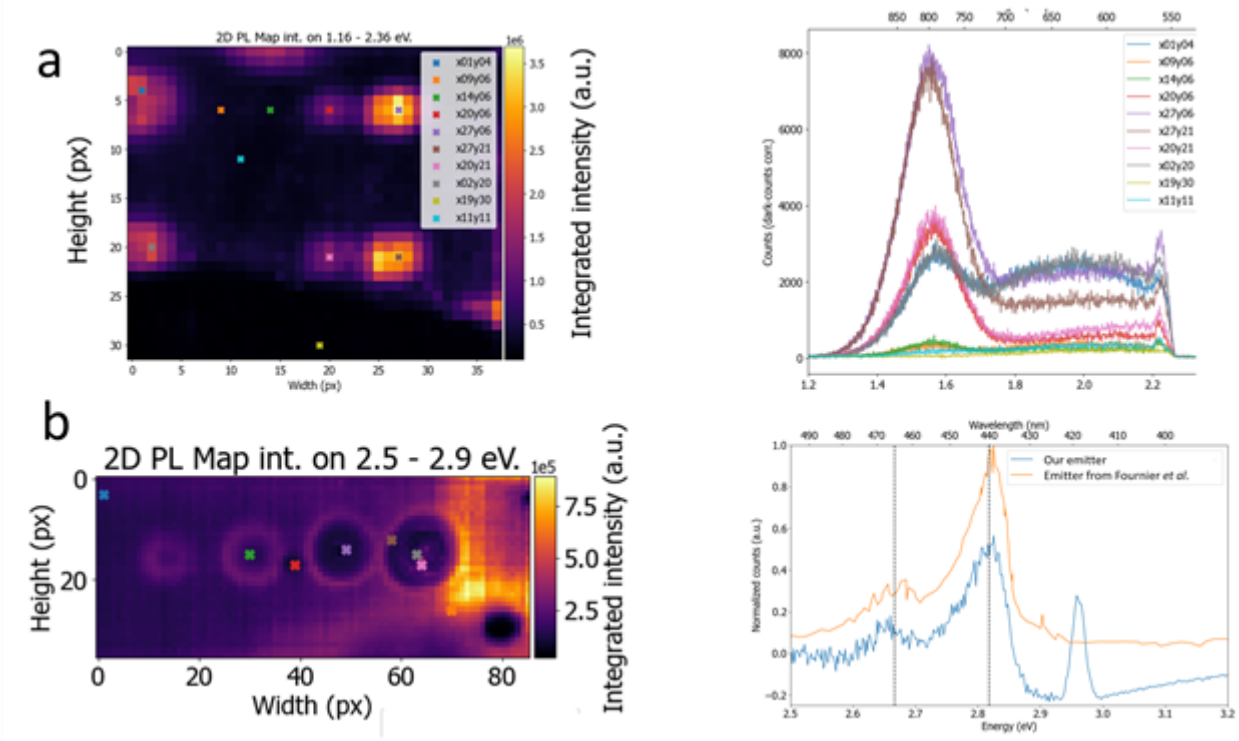

Keywords:

Irradiation Engineering; FIB; SEM

Reference:

1. Zabelotsky, T. et al. Creation of Boron Vacancies in Hexagonal Boron Nitride Exfoliated from Bulk Crystals for Quantum Sensing. ACS Appl Nano Mater 6, 21671–21678 (2023).
2. Fournier, C. et al. Position-controlled quantum emitters with reproducible emission wavelength in hexagonal boron nitride. Nat Commun 12, (2021).